



# High-yield, automated intracellular electrophysiology in retinal pigment epithelia

Colby F. Lewallen<sup>a,\*</sup>, Qin Wan<sup>b</sup>, Arvydas Maminishkis<sup>b</sup>, William Stoy<sup>c</sup>, Ilya Kolb<sup>c,d</sup>, Nathan Hotaling<sup>b</sup>, Kapil Bharti<sup>b</sup>, Craig R. Forest<sup>a</sup>

<sup>a</sup> Georgia Institute of Technology, G.W. Woodruff School of Mechanical Engineering, Atlanta, GA 30332, USA

<sup>b</sup> National Eye Institute, National Institutes of Health, Bethesda, MD 20892, USA

<sup>c</sup> Georgia Institute of Technology, Wallace H Coulter Department of Biomedical Engineering, Atlanta, GA 30332, USA

<sup>d</sup> HHMI Janelia Research Campus, Howard Hughes Medical Institute, Ashburn VA 20147, USA

## ARTICLE INFO

### Keywords:

Intracellular electrophysiology  
Sharp pipette  
Epithelia  
Automation

## ABSTRACT

**Background:** Recent advancements with induced pluripotent stem cell-derived (iPSC) retinal pigment epithelium (RPE) have made disease modeling and cell therapy for macular degeneration feasible. However, current techniques for intracellular electrophysiology – used to validate epithelial function – are painstaking and require manual skill; limiting experimental throughput.

**New Method:** A five-stage algorithm, leveraging advances in automated patch clamping, systematically derived and optimized, improves yield and reduces skill when compared to conventional, manual techniques.

**Results:** The automated algorithm improves yield per attempt from 17% (manually,  $n = 23$ ) to 22% (automated,  $n = 120$ ) (chi-squared,  $p = 0.004$ ). Specifically for RPE, depressing the local cell membrane by  $6\ \mu\text{m}$  and electroporating (buzzing) just prior to this depth ( $5\ \mu\text{m}$ ) maximized yield.

**Comparison with Existing Method:** Conventionally, intracellular epithelial electrophysiology is performed by manually lowering a pipette with a micromanipulator, blindly, towards a monolayer of cells and spontaneously stopping when the magnitude of the instantaneous measured membrane potential decreased below a pre-determined threshold. The new method automatically measures the pipette tip resistance during the descent, detects the cell surface, indents the cell membrane, and briefly buzzes to electroporate the membrane while descending, overall achieving a higher yield than conventional methods.

**Conclusions:** This paper presents an algorithm for high-yield, automated intracellular electrophysiology in epithelia; optimized for human RPE. Automation reduces required user skill and training while, simultaneously, improving yield. This algorithm could enable large-scale exploration of drug toxicity and physiological function verification for numerous kinds of epithelia.

## 1. Introduction

The retinal pigment epithelium (RPE) is a single layer of highly specialized cells in the back of the vertebrate eye that perform numerous functions that are essential for maintaining the health and integrity of the retina. In particular, RPE are responsible for the transport of ions, metabolites, and fluid between the neural retina and the choriocapillaris (Campbell and Humphries, 2013; Jones et al., 2017; Joseph and Miller, 1991). The disruption of RPE structure or function is implicated in several forms of retinal degeneration. For instance, age related macular degeneration (AMD), the most prevalent form of blindness in elderly people over 60, is caused by atrophy of the RPE

(Bhutto and Luty, 2012; Bird, 2010, 1992; Jones et al., 2017; Klein et al., 2011; Lim et al., 2012; Wong et al., 2014). Several commonly used drugs including anti-malaria drug (Chloroquine (Parikh et al., 2016)), glaucoma drug (Latanoprost (Makri et al., 2017)), anti-allergy drug (Epinephrine), multiple sclerosis drugs (Corticosteroids and Fingolimod (Heath et al., 2017)), and anti-cancer drugs (MEK-inhibitors – Pimasertib, Trametinib, Binimetinib, Cobimetinib, and Selumetinib (Montana and Apte, 2017)) increase the chance of developing sight-threatening conditions such as macular edema and retinal detachment, perhaps by disrupting channel/transporter function in the RPE and inhibiting fluid transport.

No cure for macular degenerative diseases exist, yet promisingly,

\* Corresponding author.

E-mail address: [clewallen3@gatech.edu](mailto:clewallen3@gatech.edu) (C.F. Lewallen).

<https://doi.org/10.1016/j.jneumeth.2019.108442>

Received 2 April 2019; Received in revised form 20 September 2019; Accepted 24 September 2019

Available online 25 September 2019

0165-0270/© 2019 Published by Elsevier B.V.

recent phase-I clinical trials using a monolayer of human embryonic stem cell (hESC)-derived RPE, transplanted in the sub-retinal space (SRS), have demonstrated some signs of visual recovery in humans suffering from severe exudative (wet) and late-stage (dry) AMD (Da Cruz et al., 2018; Jones et al., 2017; Kashani et al., 2018; Wong et al., 2014). In addition, recent studies utilizing an induced pluripotent stem cell (iPSC)-derived RPE patch, also transplanted in the SRS, have demonstrated anatomical and functional recovery of damaged photoreceptors in a pig model with laser-induced RPE injury (Sharma et al., 2019). For therapeutic use, iPSC and hESC-derived RPE health and function must be verified using a variety of metrics such as: gene/protein expression and electrophysiology of the cells in an intact monolayer (Miyagishima et al., 2016; Sharma et al., 2019). This latter metric, electrophysiology, is used to quantify epithelia responses to physiologically relevant stimuli.

For example, in the intact cat eye, it has been shown that the transition between light and dark environments causes a drop in potassium (K<sup>+</sup>) concentration in the SRS (Linsenmeier and Steinberg, 1984, 1982). This physiological condition has been simulated, *in vitro*, by artificially altering apical bath ion concentrations and observing the effects on RPE electrical responses (Hughes et al., 1988; Immel and Steinberg, 1986; la Cour et al., 1986; Miller and Steinberg, 1979). Similar *in vitro* intracellular electrophysiology assays are used to study ion permeability and disease mechanisms (e.g., cystic fibrosis) with epithelia such as tracheal, skin, mammary, respiratory, and kidney (Blaug et al., 2003, 2001; Cotton et al., 1987; Rothenberg et al., 1982; Tang et al., 1985; Welsh, 1984). Consequently, *in vitro* electrophysiology assays are a powerful tool to study underlying epithelia channel distribution patterns that can be used to study cell physiology, disease processes, and drug toxicity (Miyagishima et al., 2016).

*In vitro* epithelia electrophysiology measurements are conventionally performed in a modified Üssing chamber with separate apical and basal bath perfusion (Hughes et al., 1988; Joseph, 1992; Miller and Steinberg, 1977). To perform the measurement intracellularly, a sharp glass pipette, approximately 100–200 nm in diameter at the tip (validated with scanning electron microscopy (SEM)), must be delicately positioned and inserted, blindly, into the cell's cytoplasm, termed "break in" (Maminishkis et al., 2006).

In conventional, manual experiments, the pipette is mounted in a pipette holder that is rigidly connected to a microelectrode amplifier that is attached to the translating stage of a piezoelectric motor. To initiate pipette descent towards the tissue, a user must continuously press a button on a custom-made instrument. When the button is pressed, the pipette rapidly descends towards the cell monolayer, and spontaneously stops movement when detecting a voltage decrease that exceeds a predetermined threshold. However, in some cases, no voltage drop is detected during descent (e.g., the pipette tip was clogged, or it penetrated the cell tight junction rather than the cytoplasm). In these cases, the pipette will likely puncture a hole in the RPE monolayer. If a hole is created, the entire tissue needs to be discarded because it creates an electrical 'short-circuit' across the monolayer; allowing for the free exchange of ions between the apical and basal baths. The free exchange of ions between baths can alter the measured electrical properties enough to contaminate the results of subsequent experiments. Therefore, manual experiments require a trained user to closely monitor an oscilloscope and determine when to halt the translation of the pipette and avoid tissue damage.

Visual guidance of the pipette under microscopy could ameliorate the issues with manual intracellular recordings and would enable stable and high-quality recordings, but visual guidance would significantly complicate the modified Üssing chamber setup due to a lack of space for a microscope lens – with sufficient magnification – and an opposing light source. Thus, the pipette insertion process must be performed without conventional optical feedback techniques (Juusola et al., 2016). As a result, intracellular electrophysiology of epithelia is something of an art form, requiring great skill and years of training, and

thus has been limited to isolated laboratory studies on carefully selected cells and drugs (Bialek and Miller, 1994; Blaug et al., 2003, 2001; Cotton et al., 1987; Hernandez et al., 1995; Hu et al., 1996; Kokkinaki et al., 2011; Maminishkis et al., 2006; Miyagishima et al., 2016; Quinn and Miller, 1992; Rothenberg et al., 1982; Tang et al., 1985; Welsh, 1984). For *in vitro* intracellular electrophysiology of epithelia to become a broadly accepted technique for high-quality validation of cell-replacement therapies and drug screening, it must achieve higher yield and require less technical skill.

Automation of whole-cell patch clamp recording of neurons in the living brain has been reported previously (Kodandaramaiah et al., 2012). The resulting "autopatching" robot automatically establishes electrical and molecular connections to individual cells embedded in intact tissue using a glass pipette, thus enabling electrical recordings. Despite differences in cell preparation, pipette geometry, chemistry, and recording methodology, we were inspired to explore whether we could recast such a technique to suit sharp glass pipette intracellular electrophysiology of epithelial cells.

Once cells are detected using an algorithm that monitors pipette resistance changes as it approaches the epithelia, subsequent algorithms to break in and record in a high-yield and automated fashion were developed. After implementation and optimization with RPE, we report a five-stage algorithm that achieves a 74% break in success rate, and a 22% stable recording yield (n = 120) compared to 44% and 17% (n = 23) for a skilled user, respectively. This algorithm improves the stable recording yield of a skilled user (chi-squared, p = 0.004), but, unlike the conventional technique, requires virtually no user training or skill.

## 2. Materials and methods

### 2.1. Primary hfrPE cell culture

We used previously published protocols for culturing human fetal RPE (hfrPE) (Maminishkis et al., 2006). Briefly, hfrPE were isolated from fetal eyes at 16–18 weeks gestation (Advanced Bioscience Resources, Alameda, CA) and cultured in Primaria® tissue culture flasks (BD Biosciences, Franklin Lakes, NJ). Culture medium was changed every 3 days and cells were subcultured with a trypsin-EDTA treatment and seeded on semipermeable Transwells (Corning Costar). Only cells of passage 1 were used for all studies. The experiments were usually performed after 6–8 weeks of culture or after the cells formed a completely confluent monolayer. Confluence was determined by observing uniform, pigmented coverage of the Transwell and when the tissue transepithelial resistance (TER) was greater than 300 Ω·cm<sup>2</sup> (Miyagishima et al., 2016). All cells were maintained on Transwells at 37 °C in a 5% CO<sub>2</sub> humidified incubator with medium change 3 times per week.

### 2.2. Generation, differentiation, and characterization of human iPSC-RPE

Cells, isolated from donor tissue, were reprogrammed using Sendai virus-mediated delivery (CytoTune, Life Technologies) of the four Yamanaka factors (c-MYC, KLF4, OCT4, and SOX2), following the manufacturer's recommendations. Three-germ layer differentiation of iPSC lines were performed using a published protocol (Takahashi et al., 2009). Antibodies against NESTIN, TUJ1, SOX17, AFP, BRACHYURY, and SMA were used for characterization of cells of all three germ layers. Karyotyping was performed at Cell Line Genetics (Madison, WI). iPSCs were differentiated into RPE using a previously published protocol (Ferrer et al., 2014) with modifications (Sharma et al., 2019). Differentiated RPE cells were characterized by transmission electron microscopy (TEM) for morphology, gene expression, and immunostaining for RPE specific markers. All human work was done under institutional review board-approved protocol #11-E1-0245.

### 2.3. Pipette fabrication

Sharp microelectrode pipettes were pulled from 1 mm outer diameter, 0.5 mm inner diameter, fire-polished borosilicate glass with a filament (Sutter Instruments) on a P-97 puller with a 2.5 x 2.5 mm box filament (Sutter Instrument). The pipettes were pulled in a single cycle of the puller. The resulting pipette has a tip size approximately 100–200 nm in diameter (validated with SEM), resistance between 100–150 M $\Omega$ , and a voltage offset magnitude no greater than 12 mV.

### 2.4. Cell culture medium and physiology solution compositions

Methods were originally developed by Maminishkis et al. (Maminishkis et al., 2006), and are briefly summarized here. MEM- $\alpha$  modified medium (Sigma-Aldrich) was used to formulate 5% and 15% serum-containing media for culturing RPE cells. The solution contained fetal bovine serum (Atlanta Biologicals), N1 supplement (Sigma-Aldrich) 1:100 mL/mL, glutamine-penicillin-streptomycin (Sigma-Aldrich) 1:100 mL/mL, and nonessential amino acid solution (Sigma-Aldrich) 1:100 mL/mL.

The bulk Ringer solution, used in electrophysiology experiments, consisted of 5 mM KCl, 116.5 mM NaCl, 23 mM NaHCO<sub>3</sub>, 0.5 mM MgCl<sub>2</sub>, 1.8 mM CaCl<sub>2</sub>, 2 mM taurine, 5 mM glucose, and 10 mM sucrose. The Ringer solution was bubbled with 5% CO<sub>2</sub>, 10% O<sub>2</sub>, and 85% N<sub>2</sub> to bring the Ringer solution to a pH near 7.4 and an osmolarity 295  $\pm$  5 mOsm. 1 mM K<sup>+</sup> Ringer solution was prepared using the same recipe except for isosmotic substitution of NaCl for decreased KCl.

### 2.5. Tissue preparation

Prior to an experiment, a 7 mm circular section of the RPE culture was cut out with a punch (Acuderm inc.), then placed on a supporting nylon mesh to increase the monolayer stiffness, reduce the magnitude of oscillation due to fluctuations and bubbles of the perfusion solution, and maximize measured tissue resistance. The RPE was placed – apical side up – in between the two halves of a modified Üssing chamber (Miller and Steinberg, 1977). The two halves of the modified Üssing chamber were sealed to create physical and electrochemical separation of RPE apical and basolateral membranes. To ensure this seal, a thin layer of silicone vacuum grease (Beckman Coulter), was applied, by hand, to the inner side of the chamber halves. The chamber is depicted in Fig. 1.

Fig. 1 shows how the pipette accesses the RPE from the apical side while it is flanked by a pair of agar bridges (connected to Calomel electrodes), as well as Ag/AgCl working and counter electrodes placed

in the apical and basal halves, respectively. Perfusion inlets deliver the apical and basal Ringer solution to the RPE through ports machined in the modified Üssing chamber. Perfusion outlets remove Ringer solution through vacuum lines positioned so that fluid height, and, consequently, fluid pressure remains constant across the RPE membrane. The modified Üssing chamber was rotated approximately 30 degrees from horizontal.

### 2.6. Electrophysiology experiments

Some of the hardware used for RPE electrophysiology was based on the previously reported apparatus for automated patch clamp electrophysiology (Kodandaramaiah et al., 2016). A Multiclamp 700B (Molecular Devices) amplifier was utilized to amplify measured membrane potentials. Signals were acquired with a NI USB-6211 (National Instruments) and processed in LabView 2016 at 50 Hz (National Instruments). A combination of a 3-axis, MP-285 micromanipulator (Sutter Instrument) with a PT1-Z8 Motorized Translation Stage (Thorlabs), and 1 mm pipette holder (Molecular Devices) were used to constrain and translate the pipette. The pipette was backfilled with 150 mM KCl solution.

Calomel electrodes, in series with agar bridges, were connected to the apical and basal Ringer solution baths (See Fig. 1) to measure the voltage across the RPE monolayer. The voltage difference across the RPE monolayer is commonly referred to as transepithelial potential (TEP). Transepithelial resistance (TER), which includes 3 parallel resistors (cellular resistance, resistance between adjoining cells at tight-junctions, and the resistance between the tissue and chamber walls), was determined by sending one period of a symmetrical square wave ( $\Delta I = 1 \mu A$ , period = 3 s) every 40 s, measuring the corresponding change in TEP ( $\Delta TEP$ ), and inserting these values into Ohm's law:  $TER = \Delta TEP / \Delta I$ .

The pipette, once inserted into the cytoplasm of a single RPE, measures the voltage potential between the pipette and the basal reference electrode (see Fig. 1); referred to as the basal membrane potential ( $V_B$ ). The apical membrane potential ( $V_A$ ) was calculated by rearranging the TEP equation:  $V_A = V_B - TEP$ .

Continuous perfusion across both the apical and basal side of the RPE must be electrically isolated from the source to the waste collection flask to prevent an electrical short circuit. Perfusion was gravity driven and the flow rate was adjusted with a threaded tube clamp. Perfusion rates were determined as described in previous work (Maminishkis et al., 2002). Bubbles were reduced in the modified Üssing chamber by coating the chamber surface with Sigmacote hydrophobic solution (Sigma-Aldrich), and by keeping the Ringer solution temperature along

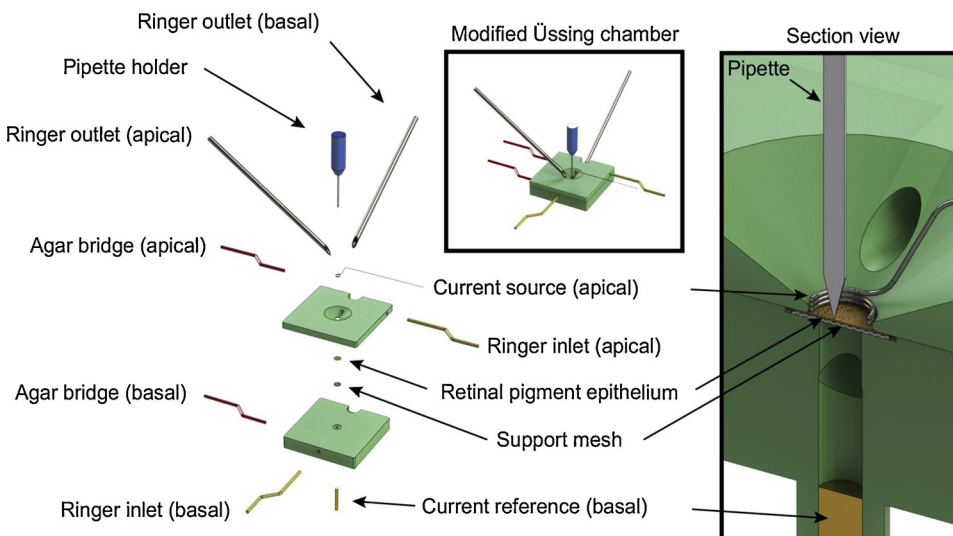


Fig. 1. Exploded view of the modified Üssing chamber used for RPE perfusion and electrophysiology. Red tubing indicates the location of the agar bridge connections to the Ringer solution. The yellow tubing indicates the location of the Ringer inlets. The silver tubing indicates the location of the vacuum lines.

the perfusion line between 35–37 °C with a custom-made water jacket around the Ringer inlets. Ringer solution was removed, after crossing the RPE tissue, with a vacuum line and deposited in one of two 1 L vacuum flasks; one flask for the apical solution and one flask for the basal solution.

Once the pipette was successfully inserted into a cell and approximately 5 min had elapsed to allow the system to reach steady state, the apical Ringer solution was replaced with a solution containing a different salt composition or pharmacological agent to induce cell physiological changes. Specifically, two unique, physiologically relevant solutions were used to assess RPE function: (1) a Ringer solution, identical to the original recipe, except that the potassium (K<sup>+</sup>) concentration was changed from 5 mM to 1 mM and (2) a Ringer solution containing 100 μM ATP. These solutions were perfused continually until the TEP began to reach a new equilibrium. Once the new equilibrium was reached, the original Ringer solution replaced the modified solution until it returned to baseline.

### 2.7. Pipette position algorithm

To initiate a recording, five discrete stages of pipette positioning were developed that compose the pipette position algorithm (see Fig. 2). In the first stage, called “Approach,” pipettes installed in the robot were localized directly above the tissue and lowered until the surface of the Ringer solution was detected. The pipette detected the surface of the solution by monitoring pipette tip resistance at 50 Hz. When the tip resistance was less than 1 GΩ, the pipette was deemed to be in the solution.

Before proceeding to the detection stage (see Fig. 2), the pipette resistance was verified to be 100–150 MΩ. If the resistance was outside this range, the pipette was discarded, and the procedure was restarted with a new pipette. If the pipette was within the resistance range, it approached the RPE apical membrane at 15 μm/s while resistance was measured continuously. The pipette resistance was measured using a 1.1 nA, 50 Hz square wave and measuring the resultant voltage amplitude. These values were used in Ohm’s law to calculate the pipette tip resistance. When the resistance difference over a 1 s rolling window exceeded 4 MΩ, the RPE apical membrane was “detected,” and the robot was paused for 3 s.

If the pipette spontaneously broke into the cell membrane during the 3 s pause and, consequently, the measured potential decreased by

more than 1 mV, the remaining break in procedure was skipped. However, if the measured potential change was less than 1 mV, a 6 μm pipette descent (60% of average cell thickness) would be initiated at maximum velocity (peak velocity during descent was ~15 μm/s) to “indent” the local apical membrane (see Fig. 2). This decent depth was optimized by measuring the yield for depths between 0–10 μm in 1 μm steps. The “buzz” command, available in current clamp mode while using the Multiclamp 700B software (Molecular Devices), was initiated after the pipette had advanced 83% (or 5 μm) of the 6 μm indent depth. Like decent depth, buzz depth was optimized by varying the location when the buzz was initiated relative to the target indent depth. Specifically, a buzz depth of 0 μm would indicate that the buzz was initiated when the pipette reached the indent depth, and a buzz depth of –1 μm would indicate that the buzz was initiated when the pipette was 1 μm above the desired indent depth. Additionally, the pipette was not paused to initiate the buzz during the indent. To reduce calcium influx, the buzz duration was set to 100 μs because it was the shortest duration that was repeatably executed by the Multiclamp 700B.

After electroporating the RPE membrane, the break in was considered successful if the measured potential decreased by more than 30 mV from the baseline for more than 1 s; indicating electrical access to the interior of the cell. Additionally, a recording was considered stable if the membrane potential was approximately  $-51 \pm 7$  mV – the typical basal membrane potential for hRPE – for more than 5 min (Hernandez et al., 1995; Hu et al., 1996; Maminishkis et al., 2006; Miyagishima et al., 2016; Quinn and Miller, 1992). The threshold for a stable recording was set at 5 min because that is the minimum duration for a complete evoked response from RPE (Joseph, 1992), and, additionally, cell loss (after the 5 min threshold) can be caused by multiple other factors not necessarily related to the cell impalement algorithm. For example, unstable or turbulent perfusion can cause small perturbations of the tissue relative to the intracellular pipette, or cell swelling and shrinking in response to the introduction of new drugs could break the tight seal at the pipette-membrane interface. In both cases, cell loss would not be related to the insertion technique.

## 3. Results and discussion

### 3.1. Break in algorithm

The break in process was systematically optimized by separating

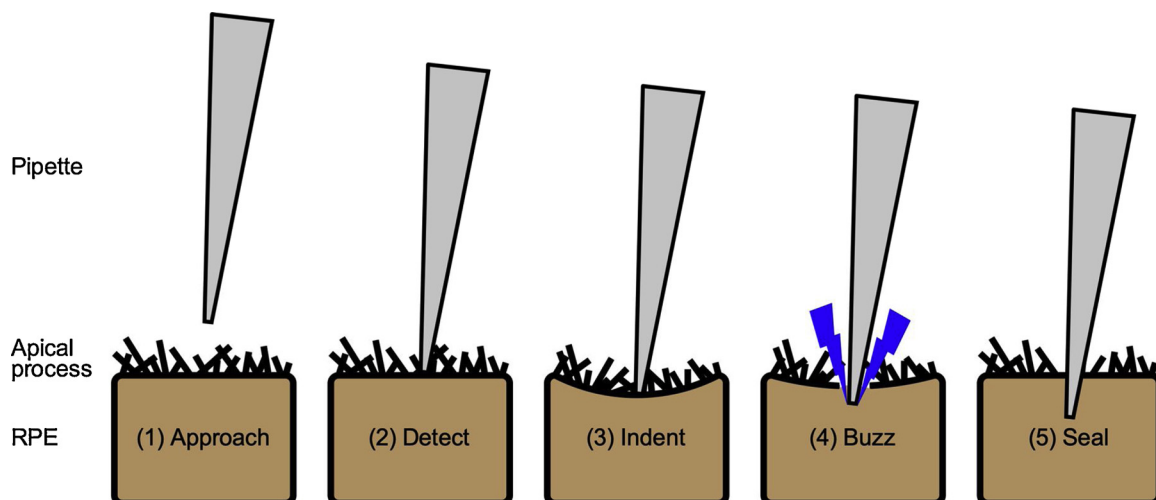


**Fig. 2.** The algorithm used to break in to RPE (from left to right). (1) “Approach” at a constant velocity while continuously monitoring tip resistance. (2) When the pipette tip resistance increase was detected, the pipette descent was paused, and the head stage was switched to current clamp mode (do not measure resistance anymore). (3) If the pipette does not spontaneously break into the RPE membrane, rapidly descend the pipette at maximum velocity to “indent” the RPE membrane. (4) While indenting the RPE membrane, send a brief “buzz” command to the head stage. (5) Check the resultant change in measured tip potential and see if the membrane “seals” around the pipette.

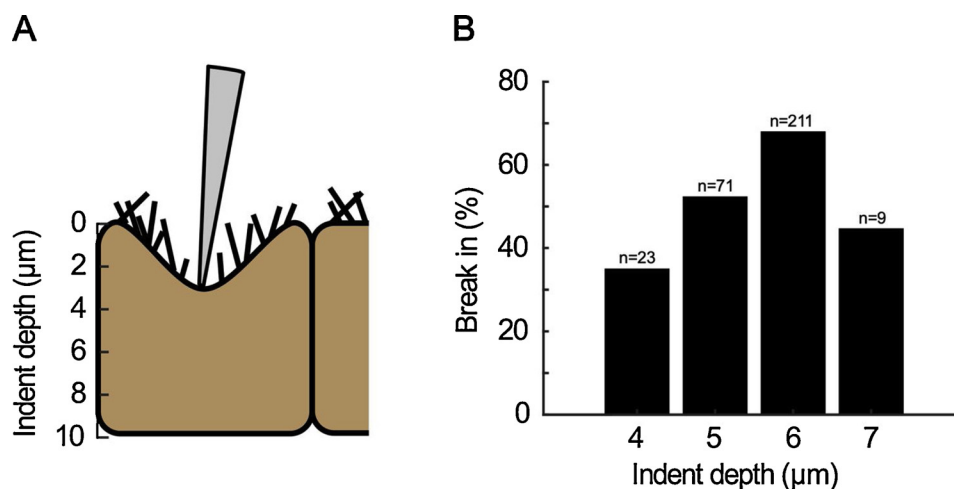


**Fig. 3.** (A) Graphical representation of the pipette and cell configuration during the indent step of the break in algorithm. (B) The probability of successful break in as a function of pipette indent depth.

into five stages (Fig. 2). In this algorithm, the buzz event occurs *prior* to the full depth of indentation and triggers a potential drop, due to break in, virtually instantaneously. The additional pipette advancement after break in seems to enhance seal yield. This observation was tested by attempting random combinations of both buzz and indent depths and observing break in yields. Break in probability was measured at 1 µm depths, as shown in Fig. 3.

Indent depths less than 4 µm did not generate enough force on the membrane to consistently break in to the RPE membrane. In addition, indent depths greater than 6 µm occasionally broke the pipette tip. This is likely because RPE monolayers are, on average, 10 µm thick at the center with a slight decrease near the extremities, and, if the pipette makes first contact near the cell junctions, could descend far enough to collide with the Transwell membrane (Lu et al., 1999). Puncturing the Transwell membrane is catastrophic for an electrophysiology experiment because it creates a hole that electrically connects the apical and basal Ringer solutions; thus, requiring complete replacement of the tissue. Thus, from Fig. 3 it was concluded that the optimum descent depth was in the range of 4–6 µm for RPE.

A chi-squared test verifies that break in chance is a function of indent depth ( $p = 0.003$ ). Regardless of buzz depth (less than or equal to indent depth), there appeared to be a maximum break in probability of 68% ( $n = 211$  trials) at an indent depth of 6 µm (60% of average RPE thickness).

The effect of relative buzz depth was evaluated as shown in Fig. 4.

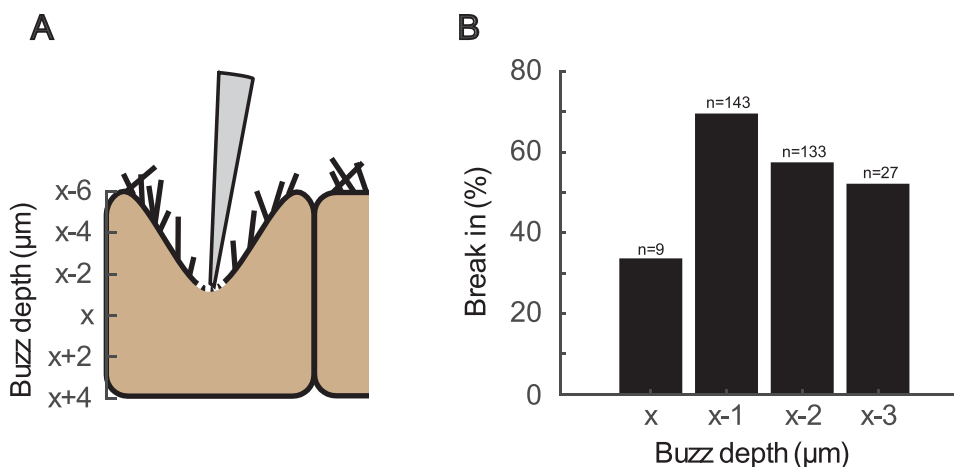


**Fig. 4.** (A) graphical representation of the pipette approximately 1 µm above a target indent depth, x. (B) the probability of successful break in as a function of relative buzz signal depth only.

**Table 1**  
Stable hRPE electrical properties reported in literature (manual) compared with values obtained with our automated method.

Method	n	V <sub>b</sub> (mV)	TEP (mV)	TER ( $\Omega \cdot \text{cm}^2$ )
(Hernandez et al., 1995)	9	$-48 \pm 6$	$3.2 \pm 1.5$	$227 \pm 90$
(Hu et al., 1996)	5	$-58 \pm 14$	$1.7 \pm 0.3$	$326 \pm 92$
(Maminishkis et al., 2006)	12	$-50 \pm 4$	$2.6 \pm 0.8^*$	$501 \pm 138^*$
(Miyagishima et al., 2016)	9	$-52 \pm 2$	$7.3 \pm 2.1$	$647 \pm 120$
Automated method	23	$-53 \pm 3$	$1.2 \pm 0.9$	$544 \pm 79$

Note: 26 stable attempts with our automated method were recorded. However, the exact magnitude of the first 3 stable recordings were not documented. Thus, we report average responses for 23/26 stable recordings using the automated method. All data are shown as mean  $\pm$  standard deviation.

\* n = 35 for TEP and TER recordings.

chamber must have a large gap between the two halves. To fill the remaining gap when mounting thinner tissues – and ensure sufficient electrical and fluid clamping around the tissue – a nylon supporting mesh is used. Consequently, the thickness of the nylon mesh is determined by maximizing the measured TER for the cell line because this is an indication of high clamping resistance at the interface between the cells and the Üssing chamber. If the nylon mesh was not sufficiently thick, the tissue could drift relative to the pipette position, negatively impacting measured yields. After optimizing the mesh thickness, indent depth, and relative buzz depth, the break in and stable recording yield for a 6  $\mu\text{m}$  indent depth and a 5  $\mu\text{m}$  buzz depth is 74% and 22% (n = 120), respectively.

### 3.2. Validation of cell health

To ensure that the new, automated insertion technique does not significantly alter the health of RPE, the electrical properties can be compared to data presented in literature (Table 1).

Statistical analysis of hRPE data presented in literature reveals a lack of agreement on what constitutes acceptable TEP and TER (p < 0.001 for both cases). The largest outlier appears to be the data presented by Miyagishima et al., 2016. However, the variance in TEP and TER can be explained by factors unrelated to tissue health or quality. For example, TEP is directly affected by the relative pressures of the apical and basal fluid which are set, by hand, prior to each experiment. In addition, the quality of the clamping force separating the apical and basal solutions is usually optimized before the experiment by maximizing the measured TER for the desired cell line; implying that clamping force and quality also plays a role in reported TER. Therefore, it seems that tissue TEP and TER would be a poor indicator of the effect that the automated insertion process has on tissue health.

In contrast to TEP and TER, V<sub>b</sub> is a cell-specific parameter and should not be drastically affected by experimental settings such as the chamber clamping force and the relative fluid pressures, and it should be more directly related to balance of ions both inside and outside the cell as governed by the Goldman-Hodgkin-Katz equation. If the electroporation process during the insertion of the electrode damages the cell, ions would spontaneously transfer in and out of the cell; drastically altering the measured membrane potential (Li et al., 2004). Therefore, V<sub>b</sub> from RPE in literature – submerged in similar extracellular Ringer's solutions – can be averaged together to give an expected resting membrane potential ( $-51 \pm 7$  mV). A two-tailed *t*-test comparing the distributions of V<sub>b</sub> reported in literature and the V<sub>b</sub> measured with the automated method reveals that they are not statistically different (p > 0.2), and it can be concluded that the automated pipette insertion process has no statistically detectable effect on tissue health.

Furthermore, the results of a complete electrophysiology experiment performed using both the optimized algorithmic methods and the original, manual method gives insight into channel function and distribution of RPE (Fig. 5).

Intracellular recordings of RPE membrane potential in response to apical low K<sup>+</sup> or ATP provide important functional assessments to authenticate RPE physiology. Altering the apical bath K<sup>+</sup> concentration from 5 to 1 mM mimics the extracellular K<sup>+</sup> concentration drop that occurs *in vivo* in the subretinal space of the eye, which is initiated by changes in photoreceptor activity following the transition from dark-to-light (Dmitriev et al., 1996; Joseph and Miller, 1991). ATP is a proposed Light Peak (LP) substrate; ATP acts on apical membrane purinergic P2Y<sub>2</sub> receptors, causing subsequent downstream signaling that leads to channel activity changes on RPE apical and basal membrane; thus, driving fluid transport across the RPE monolayer (Peterson et al., 1997). These two physiological stimuli are critical indicators of the health and integrity of the RPE monolayer.

With the automated method, in both hRPE and iPSC-RPE, the potassium concentration drop in the apical bath caused a 30 mV hyperpolarization of the RPE apical and basal membranes and 1–2 mV increase in the TEP (Fig. 5A and B). In contrast, apical ATP application on hRPE and iPSC-RPE induced about a 20 mV membrane depolarization in both membranes (Fig. 5A and B). These responses have been observed previously, using the manual method, in primary cultured hRPE and various iPSC-RPE; derived from different tissue sources and donors (Miyagishima et al., 2016). In particular, the iPSC-RPE evoked response data (Fig. 5C) shows no distinguishable difference between the automated (n = 10) and manual (n = 15) methods for each experimental condition ( $-54.6 \pm 1.5$  mV vs.  $-55.0 \pm 1.0$  for baseline,  $-29.4 \pm 1.6$  mV vs.  $-26.0 \pm 3.5$  mV for low K<sup>+</sup> response,  $20.6 \pm 1.2$  mV vs.  $18.0 \pm 1.6$  mV for ATP response; two-tailed *t*-test, p = 0.8, p = 0.3, p = 0.2, respectively) (Miyagishima et al., 2016).

## 4. Conclusions

This paper presents an optimized technique for high-yield, automated intracellular electrophysiology of epithelial cultures; such as human RPE. This technique improved break in yield from 44% to 74% and stable recording yield from 17% to 22% using conventional techniques and a five-stage algorithm, respectively. The algorithm was developed and optimized systematically, yielding optimal manipulator speeds, buzz duration, as well as buzz and indent depths. The baseline membrane potential and measured responses of RPE to low K<sup>+</sup> and ATP are indistinguishable from those measured with the manual technique which indicates that the methodology utilized by the algorithm does not alter the physiology of the epithelia. Surprisingly, advancing the pipette 60% through the RPE (6  $\mu\text{m}$ ), yet buzzing at 83% of this depth (5  $\mu\text{m}$ ) maximized yield. This technique overturns common practice in the field and improves yield at much lower operator skill level; enabling more labs to explore physiology, drug toxicity, and disease processes of epithelia. Future work could explore recent advancements in automated electrophysiology to further improve yield using techniques such as pipette swapping or pipette cleaning (Holst et al., 2019; Kolb et al., 2019).

### Funding acknowledgements

KB acknowledges NEI/NIH Intramural funds and DDIR Innovation Award/NIH. CRF acknowledges the NIH BRAIN Initiative Grant (NEI and NIMH 1-U01-MH106027-01), NIH R01NS102727, NIH Single Cell Grant 1 R01 EY023173, and the Georgia Tech Petit Institute for Bioengineering and Biosciences.

### Appendix A. Supplementary data

Supplementary material related to this article can be found, in the online version, at doi:<https://doi.org/10.1016/j.jneumeth.2019.108442>.

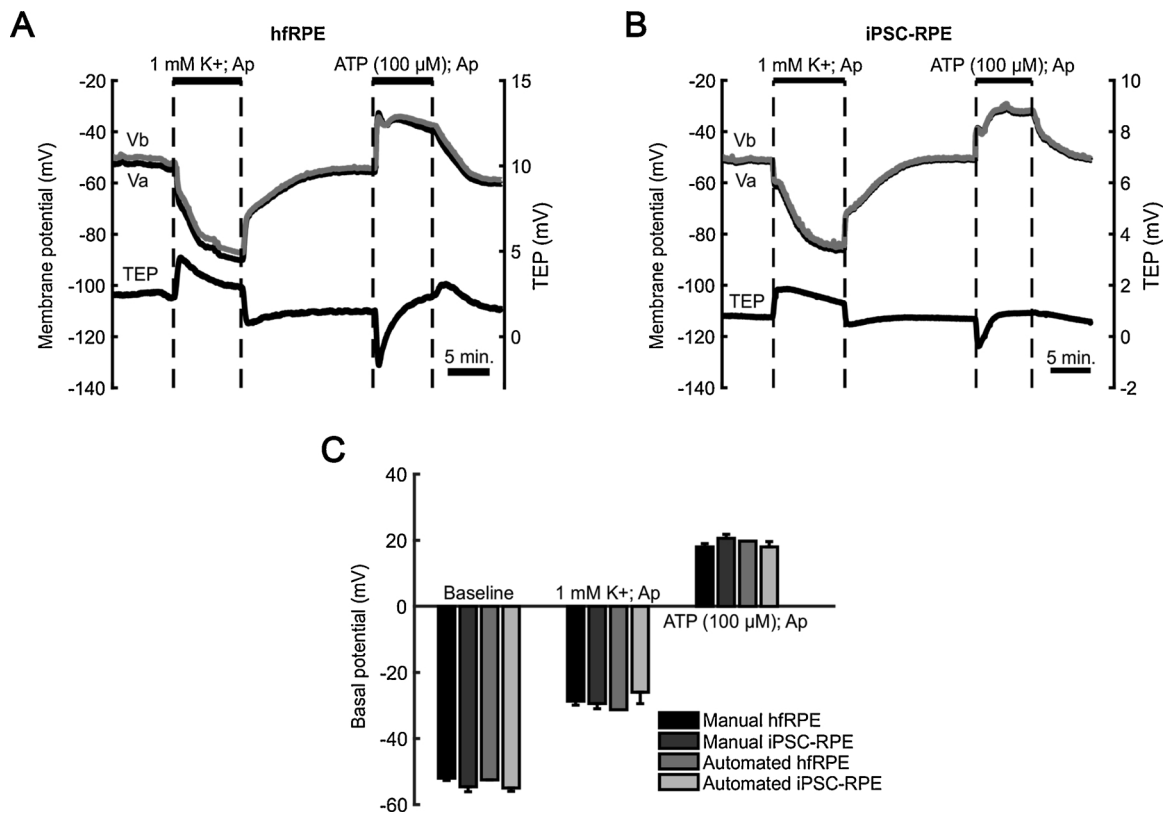


**Fig. 5.** (A and B) Representative electrical responses to apical application of low K<sup>+</sup> and ATP in cultured hfrPE (A) or iPSC-RPE (B) recorded using the automated method with optimal indent depth of 6 μm and buzz depth of 5 μm. For each graph, the top traces show the changes of apical and basal membrane potential (Va, Vb), The bottom trace shows the changes of transepithelial potential (TEP). Va, Vb, and TEP were measured simultaneously in each experiment. The black horizontal bars indicate the time during which 1 mM K<sup>+</sup> or 100 mM ATP were perfused to the apical bath. Time scale bar: 5 min. (C) Summary data for the resting and evoked Vb changes in response to low K<sup>+</sup> and ATP application using the manual or automated method. The bar chart shows the mean ± SEM of the evoked electrical responses measured using the conventional, manual technique during a previous study (hfrPE, n = 9 and iPSC-RPE, n = 15 (Miyagishima et al., 2016) and the new, automated technique (hfrPE, n = 1 and iPSC-RPE, n = 10).

## References

- Bhutto, I., Lutty, G., 2012. Understanding age-related macular degeneration (AMD): relationships between the photoreceptor/retinal pigment epithelium/Bruch's membrane/choriocapillaris complex. *Mol. Aspects Med.* 33, 295–317. <https://doi.org/10.1016/j.mam.2012.04.005>.
- Bialek, S., Miller, S.S., 1994. K<sup>+</sup> and Cl<sup>-</sup> transport mechanisms in bovine pigment epithelium that could modulate subretinal space volume and composition. *J. Physiol.* 475, 401–417. <https://doi.org/10.1113/jphysiol.1994.sp020081>.
- Bird, A.C., 2010. Review series Therapeutic targets in age-related macular disease. *J. Clin. Invest.* 120, 3033–3041. <https://doi.org/10.1172/JCI42437.tion>.
- Bird, A.C., 1992. Bruch's Membrane Change with Age. pp. 166–168. <https://doi.org/10.1136/bjo.76.3.166>.
- Blaug, S., Hybiske, K., Cohn, J., Firestone, G.L., Machen, T.E., Miller, S.S., 2001. ENaC- and CFTR-dependent ion and fluid transport in mammary epithelia. *Am. J. Physiol. Physiol.* 281, C633–C648. <https://doi.org/10.1152/ajpcell.2001.281.2.C633>.
- Blaug, S., Rymer, J., Jalickee, S., Miller, S.S., 2003. P2 purinoceptors regulate calcium-activated chloride and fluid transport in 31EG4 mammary epithelia. *Am. J. Physiol. Physiol.* 284, C897–C909. <https://doi.org/10.1152/ajpcell.00238.2002>.
- Campbell, M., Humphries, P., 2013. *The Blood-Retina Barrier*. Springer, New York, NY, pp. 70–84. [https://doi.org/10.1007/978-1-4614-4711-5\\_3](https://doi.org/10.1007/978-1-4614-4711-5_3).
- Cotton, C.U., Stutts, M.J., Knowles, M.R., Gatzky, J.T., Boucher, R.C., 1987. Abnormal apical cell membrane in cystic fibrosis respiratory epithelium. An in vitro electrophysiological analysis. *J. Clin. Invest.* 79, 80–85. <https://doi.org/10.1172/JCI112812>.
- Da Cruz, L., Fynes, K., Georgiadis, O., Kerby, J., Luo, Y.H., Ahmado, A., Vernon, A., Daniels, J.T., Nommiste, B., Hasan, S.M., Gooljar, S.B., Carr, A.J.F., Vugler, A., Ramsden, C.M., Bictash, M., Fenster, M., Steer, J., Harbinson, T., Wilbrey, A., Tufail, A., Feng, G., Whitlock, M., Robson, A.G., Holder, G.E., Sago, M.S., Loudon, P.T., Whiting, P., Coffey, P.J., 2018. Phase 1 clinical study of an embryonic stem cell-derived retinal pigment epithelium patch in age-related macular degeneration. *Nat. Biotechnol.* 36, 1–10. <https://doi.org/10.1038/nbt.4114>.
- Dmitriev, A.V., Govardovskii, V.I., Steinberg, R.H., 1996. Light-induced changes of principal extracellular ions, and the extracellular space volume in the chick retina. *Investig. Ophthalmol. Vis. Sci.* 37, 1157–1167.
- Ferrer, M., Corneo, B., Davis, J., Wan, Q., Miyagishima, K.J., King, R., Maminishk, A., Marugan, J., Sharma, R., Shure, M., Temple, S., Miller, S., Bharti, K., 2014. A multiplex high-throughput gene expression assay to simultaneously detect disease and functional markers in induced pluripotent stem cell-derived retinal pigment epithelium. *Stem Cells Transl. Med.* 3, 911–922. <https://doi.org/10.5966/sctm.2013-0192>.
- Heath, G., Airody, A., Gale, R.P., 2017. The Ocular Manifestations of Drugs Used to Treat Multiple Sclerosis. *Drugs* 77, 303–311. <https://doi.org/10.1007/s40265-017-0692-6>.
- Hernandez, E.V., Hu, J.G., Frambach, D.A., Gallemore, R.P., 1995. Potassium conductances in cultured bovine and human retinal pigment epithelium. *Investig. Ophthalmol. Vis. Sci.* 36, 113–122.
- Holst, G., Stoy, W.A., Yang, B., Kolb, I., Kodandaramaiah, S.B., Li, L., Knoblich, U., Zeng, H., Haider, B., Boyden, E.S., Forest, C.R., 2019. Autonomous patch clamp robot for functional characterization of neurons in vivo: development and application to mouse visual cortex. *J. Neurophysiol.* 2341–2357. <https://doi.org/10.1152/jn.00738.2018>.
- Hu, J.G., Gallemore, R.P., Bok, D., Frambach, D.A., 1996. Chloride transport in cultured fetal human retinal pigment epithelium. *Exp. Eye Res.* 62, 443–448. <https://doi.org/10.1006/exer.1996.0049>.
- Hughes, B.A., Miller, S.S., Joseph, D.P., Edelman, J.L., 1988. cAMP stimulates the Na<sup>+</sup> + K<sup>+</sup> pump in frog retinal pigment epithelium. *Am. J. Physiol.* 254, C84–98.
- Immel, J., Steinberg, R.H., 1986. Spatial buffering of K<sup>+</sup> by the retinal pigment epithelium in frog. *J. Neurosci.* 6, 3197–3204.
- Jones, M.K., Lu, B., Girman, S., Wang, S., 2017. Cell-based therapeutic strategies for replacement and preservation in retinal degenerative diseases. *Prog. Retin. Eye Res.* 58, 1–27. <https://doi.org/10.1016/j.preteyeres.2017.01.004>.
- Joseph, D.P., 1992. Alpha-1-adrenergic modulation of K and Cl transport in bovine retinal pigment epithelium. *J. Gen. Physiol.* 99, 263–290. <https://doi.org/10.1085/jgp.99.2.263>.
- Joseph, D.P., Miller, S.S., 1991. Apical and basal membrane ion transport mechanisms in bovine retinal pigment epithelium. *J. Physiol.* 435, 439–463.
- Juusola, M., Dau, A., Zheng, L., Rien, D., 2016. Electrophysiological method for recording intracellular voltage responses of *Drosophila* photoreceptors and interneurons to light stimuli in vivo. *J. Vis. Exp.* 1–16. <https://doi.org/10.3791/54142>.
- Kashani, A.H., Lebkowski, J.S., Rahhal, F.M., Avery, R.L., Salehi-Had, H., Dang, W., Lin, C.-M., Mitra, D., Zhu, D., Thomas, B.B., Hikita, S.T., Pennington, B.O., Johnson, L.V., Clegg, D.O., Hinton, D.R., Humayun, M.S., 2018. A bioengineered retinal pigment epithelial monolayer for advanced, dry age-related macular degeneration. *Sci. Transl. Med.* 10. <https://doi.org/10.1126/scitranslmed.aao4097>. eao4097.
- Klein, R., Chou, C., BK, K., Zhang, X., SM, M., JB, S., 2011. Prevalence of age-related macular degeneration in the us population. *Arch. Ophthalmol.* 129, 75–80.

- Kodandaramaiah, S.B., Franzesi, G.T., Chow, B.Y., Boyden, E.S., Forest, C.R., 2012. Automated whole-cell patch-clamp electrophysiology of neurons in vivo. *Nat. Methods* 9, 585–587. <https://doi.org/10.1038/nmeth.1993>.
- Kodandaramaiah, S.B., Holst, G.L., Wickersham, I.R., Singer, A.C., Franzesi, G.T., McKinnon, M.L., Forest, C.R., Boyden, E.S., 2016. Assembly and operation of the autopatcher for automated intracellular neural recording in vivo. *Nat. Protoc.* 11, 634–654. <https://doi.org/10.1038/nprot.2016.007>.
- Kokkinaki, M., Sahibzada, N., Golestaneh, N., 2011. Human iPS-derived retinal pigment epithelium (RPE) cells exhibit ion transport, membrane potential, polarized VEGF secretion and gene expression pattern similar to native RPE. *Stem Cells* 29, 825–835. <https://doi.org/10.1002/stem.635>.
- Kolb, I., Landry, C.R., Yip, M.C., Lewallen, C.F., Stoy, W.A., Lee, J., Felouzis, A., Yang, B., Boyden, E.S., Rozell, C.J., Forest, C.R., 2019. PatcherBot: a single-cell electrophysiology robot for adherent cells and brain slices. *J. Neural Eng.* 16, 046003. <https://doi.org/10.1088/1741-2552/ab1834>.
- la Cour, M., Lund-Andersen, H., Zeuthen, T., 1986. Potassium transport of the frog retinal pigment epithelium: autoregulation of potassium activity in the subretinal space. *J. Physiol.* 375, 461–479. <https://doi.org/10.1113/jphysiol.1986.sp016128>.
- Li, W.C., Soffe, S.R., Roberts, A., 2004. A direct comparison of whole cell patch and sharp electrodes by simultaneous recording from single spinal neurons in frog tadpoles. *J. Neurophysiol.* 92, 380–386. <https://doi.org/10.1152/jn.01238.2003>.
- Lim, L.S., Mitchell, P., Seddon, J.M., Holz, F.G., Wong, T.Y., 2012. Age-related macular degeneration. *Lancet* 379, 1728–1738. [https://doi.org/10.1016/S0140-6736\(12\)60282-7](https://doi.org/10.1016/S0140-6736(12)60282-7).
- Linsenmeier, R.A., Steinberg, R.H., 1984. Effects of hypoxia on potassium homeostasis and pigment epithelial cells in the cat retina. *J. Gen. Physiol.* 84, 945–970.
- Linsenmeier, R.A., Steinberg, R.H., 1982. Origin and sensitivity of the light peak in the intact cat eye. *J. Physiol.* 331, 653–673. <https://doi.org/10.1113/jphysiol.1982.sp014396>.
- Lu, L., Kam, L., Hasenbein, M., Nyalakonda, K., Bizios, R., Göpferich, A., Young, J.F., Mikos, A.G., 1999. Retinal pigment epithelial cell function on substrates with chemically micropatterned surfaces. *Biomaterials* 20, 2351–2361. [https://doi.org/10.1016/S0142-9612\(99\)00164-7](https://doi.org/10.1016/S0142-9612(99)00164-7).
- Makri, O.E., Tsaparoni, F.N., Plotas, P., Ifantis, N., Xanthopoulou, P.T., Georgakopoulos, C.D., 2017. Cystoid macular edema associated with preservative-free latanoprost after uncomplicated cataract surgery: case report and review of the literature. *BMC Res.* <https://doi.org/10.1186/s13104-017-2448-5>. Notes 10.
- Maminishkis, A., Chen, S., Jalickee, S., Banzon, T., Shi, G., Wang, F.E., Ehalt, T., Hammer, J.A., Miller, S.S., 2006. Confluent monolayers of cultured human fetal retinal pigment epithelium exhibit morphology and physiology of native tissue. *Investig. Ophthalmology Vis. Sci.* 47, 3612. <https://doi.org/10.1167/iovs.05-1622>.
- Maminishkis, A., Jalickee, S., Blaug, S.A., Rymer, J., Yerxa, B.R., Peterson, W.M., Miller, S.S., 2002. The P2Y2 receptor agonist INS37217 stimulates RPE fluid transport in vitro and retinal reattachment in rat. *Invest. Ophthalmol. Vis. Sci.* 43, 3555–3566.
- Miller, S.S., Steinberg, R.H., 1979. Potassium modulation of taurine transport across the frog retinal pigment epithelium. *J. Gen. Physiol.* 74, 237–259. <https://doi.org/10.1085/jgp.74.2.237>.
- Miller, S.S., Steinberg, R.H., 1977. Passive ionic properties of frog retinal pigment epithelium. *J. Membr. Biol.* 36, 337–372. <https://doi.org/10.1007/BF01868158>.
- Miyagishima, K.J., Wan, Q., Corneo, B., Sharma, R., Lotfi, M.R., Boles, N.C., Hua, F., Maminishkis, A., Zhang, C., Blenkinsop, T., Khristov, V., Jha, B.S., Memon, O.S., D'Souza, S., Temple, S., Miller, S.S., Bharti, K., 2016. In pursuit of authenticity: induced pluripotent stem cell-derived retinal pigment epithelium for clinical applications. *Stem Cells Transl. Med.* 5, 1562–1574. <https://doi.org/10.5966/sctm.2016-0037>.
- Montana, C.L., Apte, R.S., 2017. MEKAnisms of a serous complication. *JAMA Ophthalmol.* <https://doi.org/10.1001/jamaophthalmol.2017.0275>.
- Parikh, V.S., Modi, Y.S., Au, A., Ehlers, J.P., Srivastava, S.K., Schachat, A.P., Singh, R.P., 2016. Nonleaking cystoid macular edema as a presentation of hydroxychloroquine retinal toxicity. *Ophthalmology* 123, 664–666. <https://doi.org/10.1016/j.ophtha.2015.09.011>.
- Peterson, W.M., Meggyesy, C., Yu, K., Miller, S.S., 1997. Extracellular ATP activates calcium signaling, ion, and fluid transport in retinal pigment epithelium. *J. Neurosci.* 17, 2324–2337.
- Quinn, R.H., Miller, S.S., 1992. Ion transport mechanisms in native human retinal pigment epithelium. *Investig. Ophthalmol. Vis. Sci.* 33, 3513–3527.
- Rothenberg, P., Reuss, L., Glaser, L., 1982. Serum and epidermal growth factor transiently depolarize quiescent BSC-1 epithelial cells. *Proc. Natl. Acad. Sci. U. S. A.* 79, 7783–7787. <https://doi.org/10.1073/PNAS.79.24.7783>.
- Sharma, R., Khristov, V., Rising, A., Jha, B.S., Dejene, R., Hotaling, N., Li, Y., Stoddard, J., Stanekwicz, C., Wan, Q., Zhang, C., Campos, M.M., Miyagishima, K.J., McGaughey, D., Villamil, R., Mattapallil, M., Stanzel, B., Qian, H., Wong, W., Chase, L., Charles, S., McGill, T., Miller, S., Maminishkis, A., Amaral, J., Bharti, K., 2019. Clinical-grade stem cell-derived retinal pigment epithelium patch rescues retinal degeneration in rodents and pigs. *Sci. Transl. Med.* 11 <https://doi.org/10.1126/scitranslmed.aat5580>. eaat5580.
- Takahashi, K., Narita, M., Yokura, M., Ichisaka, T., Yamanaka, S., 2009. Human induced pluripotent stem cells on autologous feeders. *PLoS One* 4, 2–7. <https://doi.org/10.1371/journal.pone.0008067>.
- Tang, J., Abramcheck, F.J., Van Driessche, W., Helman, S.I., 1985. Electrophysiology and noise analysis of K<sup>+</sup>-depolarized epithelia of frog skin. *Am. J. Physiol. Physiol.* 249, C421–C429. <https://doi.org/10.1152/ajpcell.1985.249.5.C421>.
- Welsh, M.J., 1984. Anthracene-9-carboxylic acid inhibits an apical membrane, chloride conductance in canine tracheal epithelium. *J. Membr. Biol.* 78, 61–71. <https://doi.org/10.1007/BF01872533>.
- Wong, W.L., Su, X., Li, X., Cheung, C.M.G., Klein, R., Cheng, C.-Y., Wong, T.Y., 2014. Global prevalence of age-related macular degeneration and disease burden projection for 2020 and 2040: a systematic review and meta-analysis. *Lancet Glob. Heal.* 2, e106–e116. [https://doi.org/10.1016/S2214-109X\(13\)70145-1](https://doi.org/10.1016/S2214-109X(13)70145-1).